mcnote:mucxxx

Front End Simulation for a Double Phase Rotation Neutrino Factory

R.B. Palmer, S. Berg, R. Fernow, J. Gallardo, H. Kirk, R. Weggel
Brookhaven National Laboratory
Y. Fukui
UCLA
C. Kim, E. Kim, G. Penn, J. Wurtele
UCB
N. Mokhov
FNAL

(Dated: May 15, 2000)

Abstract

Results are presented of a complete MARS/ICOOL simulation of a double phase rotation neutrino factory front end similar to that described in the paper of *Palmer, Johnson and Keil (PJK)*. Differences include the use of a smaller radius mercury target, repositioning of the first rf cavity to 6.3 m from the target, added field reversals in the mini cooling and long drift, and the use of *FOFO* cooling. The first phase rotation uses 6 MV/m rf at 30 MHz; the second uses a ± 0.55 MV/m induction linac. The FOFO cooling lattice is similar to that proposed at LBL, but has lower current densities. After cooling, the simulation gives a total of 0.17 muons per proton, with 0.10 muons per proton within a longitudinal acceptance cut of 140 π mm, and a transverse acceptance of 15 π mm rad. A comparison is made with the performance of similar systems with different targets, proton energy, number of phase rotations and length.

CONTENTS

LIST OF FIGURES

LIST OF TABLES

I. INTRODUCTION

The work reported here has been done within the Muon Collider Collaboration, and owes much to its many members. The scenario given is based on the work of Palmer, Johnson and Keil (PJK)[1] as discussed in the scenarios working group at Lyon [2]. The simulations used in that work (for pion production[3], MCM[4] for phase rotation, a mere estimate for bunching and an earlier version of ICOOL[5] for the cooling) contained many approximations. The current work uses the latest version of the MARS code[6] and a realistic target station configuration[7] for pion production, and *ICOOL*[5] for the rest. The system described was optimized, and the numbers and plots shown were obtained using ICOOL version 2.05. The Front End, which schematic is shown in Fig. 1, has the following components:

- A target and pion capture system consisting of a mercury target in a 20 T solenoid, with a field tapering down to 1.25 T.
- Phase rotation, in 2 stages, to reduce the muon energy spread at the expense of spreading them out over a longer time interval. The system is designed to correlate the muon polarization with time, allowing control of the relative intensity of muon and anti-electron neutrinos.
- A limited amount of cooling.

This Front End would be followed by a fast muon acceleration to 20 GeV or more, in a system of a linac and one or two recirculating linear accelerators (RLAs). The beam would

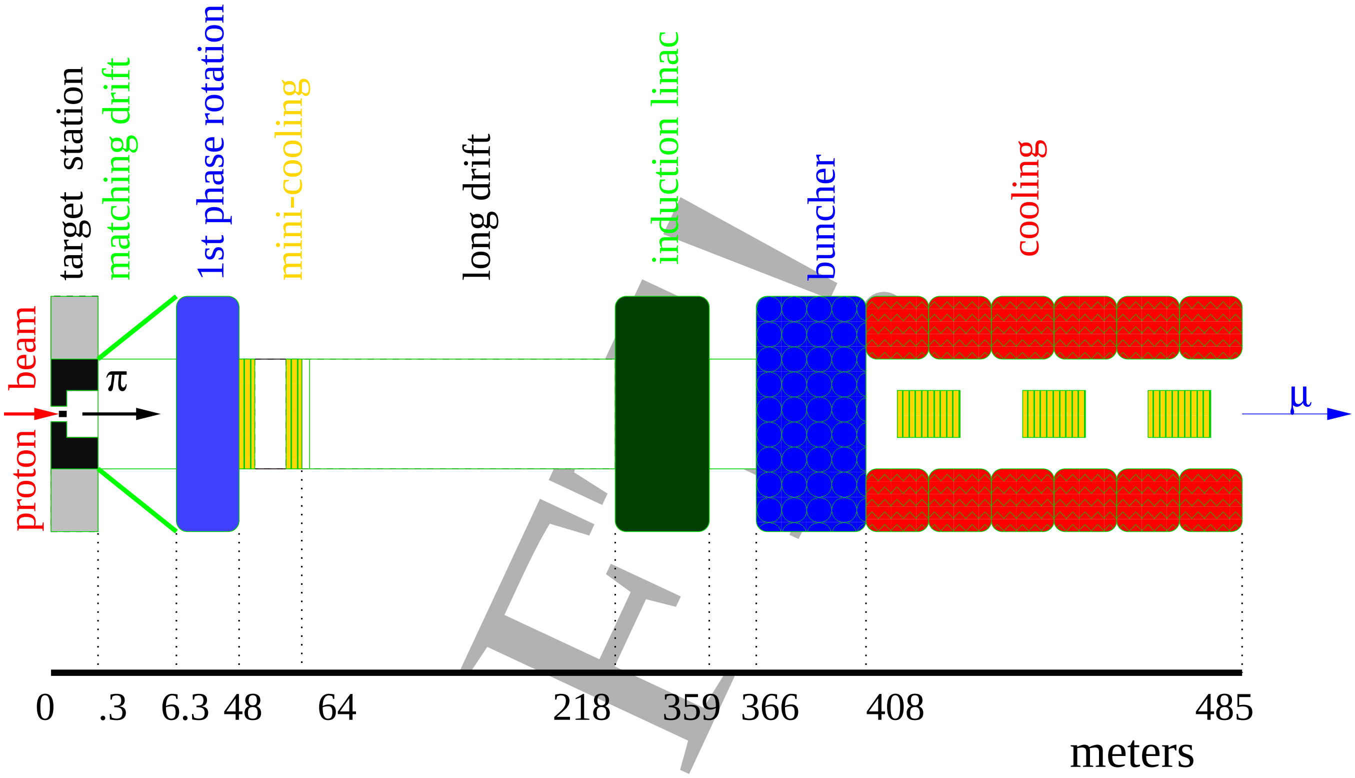

FIG. 1: Schematic of the front end

then be injected into a storage ring with long straight sections pointing to distant neutrino detectors for oscillation studies, and to one or more near detectors for high intensity studies.

A Definitions and conventions

Emittances, whether stated or not, are always taken to be the projected normalize rms values:

$$\epsilon_N = \beta_v\gamma_v\sqrt{<(x-<x>)^2><(x'-<x'>)^2> - <(x-<x>)(x'-<x'>)>^2} \qquad (1)$$

For transverse emittances x is the transverse dimension x, or y; $x' = \frac{p_x}{p_s}$ is the angle with respect to the axis in the standard accelerator coordinates system. In the longitudinal direction, x is the axial distance of the particles from the bunch center z, and x' is the dimensionless momentum difference from the average momentum, divided by the average $x' \equiv \frac{(p-<p>)}{<p>}$.

Thus, ignoring correlations:

$$\epsilon_n = \beta_v \gamma_v \sigma_x \sigma_{x'} \tag{2}$$

Another definition of emittance that is often used, corresponds to the determinant of the covariant matrix

$$\epsilon_N = \frac{[\det \mathbf{M}]^{1/6}}{m_\mu} \tag{3}$$

Acceptances are defined in terms of amplitude parameters J, the definition of which, ignoring correlations, are:

$$J_\perp = \beta_v \gamma_v \frac{\frac{x^2}{\beta} + x'^2\beta + \frac{y^2}{\beta} + y'^2\beta}{4} \tag{4}$$

$$J_{||} = \beta_v \gamma_v \frac{\frac{z^2}{\beta_s} + (\frac{dp}{p})^2\beta_s}{2} \tag{5}$$

where β is the Twiss betatron beta function and β_s is the synchrotron beta function $\beta_s = \sigma_z/(\sigma_p/p)$. The lack of correlations means that the Twiss α's are zero in all dimensions. With this convention, the average of the J's are equal to the normalized emittances. The average of any one term would gives the emittance, hence the number in the denominator equals the number of terms. Note that the x and y amplitudes are combined to correspond to circular apertures, but the definitions are for the normally defined separate x and y emittances.

The hard emittance cuts used in this paper are: $4J_\perp \approx 0.0935$ and 0.015 π m-rad transversely and $2J_{||} \approx 0.140$ π m longitudinally.

II. COMPONENTS

A Proton Source

The following table gives the assumed parameters of the 24 GeV proton driver. It includes those for a potential upgrade to 4 MW, and those for 16 GeV drivers at 1 and 4 MW.

TABLE I: Parameters of proton drivers at BNL and Fermilab.

	AGS-BNL	AGS-BNL	FermiLab	FermiLab
Energy (GeV)	24	24	16	16
Power (MW)	1	4	1	74
Repetition (Hz)	2.5	5	15	15
p's/fill	10^{14}	$2\ 10^{14}$	$2.5\ 10^{13}$	10^{14}
bunches	6	6	4	4
circumference (m)	807	807	474	474
spacing (m)	135	135	118	118
σ_t (ns)	1	1	1	1

B Target and Capture

It is assumed here that the target is a jet of liquid mercury. Pion production from the target, assumed in a 20 T uniform solenoidal field, was calculated with the MARS code[6] and written to a file at the target end. The events in this file, from 100,000 protons, have weights varying over several orders of magnitude and can cause larger statistical errors than given by normal statistics. Thus this file is used to generate a shorter file containing typically between 5000 to 15000 uniformly weighted events, and this file is used as input to ICOOL[5] for the rest of the simulation.

The dimensions and angle of the target were obtained from an optimization performed by H. Kirk[8]. The MARS code also calculates the energy deposition on the target by the macro pulse; this is shown in Fig. 2. The calculated temperature rise in such a target, for the AGS 1 MW case, assuming constant specific heat $C_p = 0.138 \frac{\mathrm{J}}{\mathrm{g}^\circ\mathrm{C}}$, is $\approx 3800\,^\circ$C. It is clear that the assumption of constant specific heat is not correct, but the number serves to indicate a likely rapid evaporation of the jet. If such evaporation occurs before the end of the spill ($2\,\mu s$ for the AGS case) then the target efficiency for the later bunches may be very low. Possible solutions to this problem are discussed in the last section. The situation is

TABLE II: Target: parameters of the liquid mercury jet

material	Hg
radius (mm)	5
length (m)	0.3
angle (rad)	0.15
solenoid field (T)	20
solenoid radius (cm)	7.5

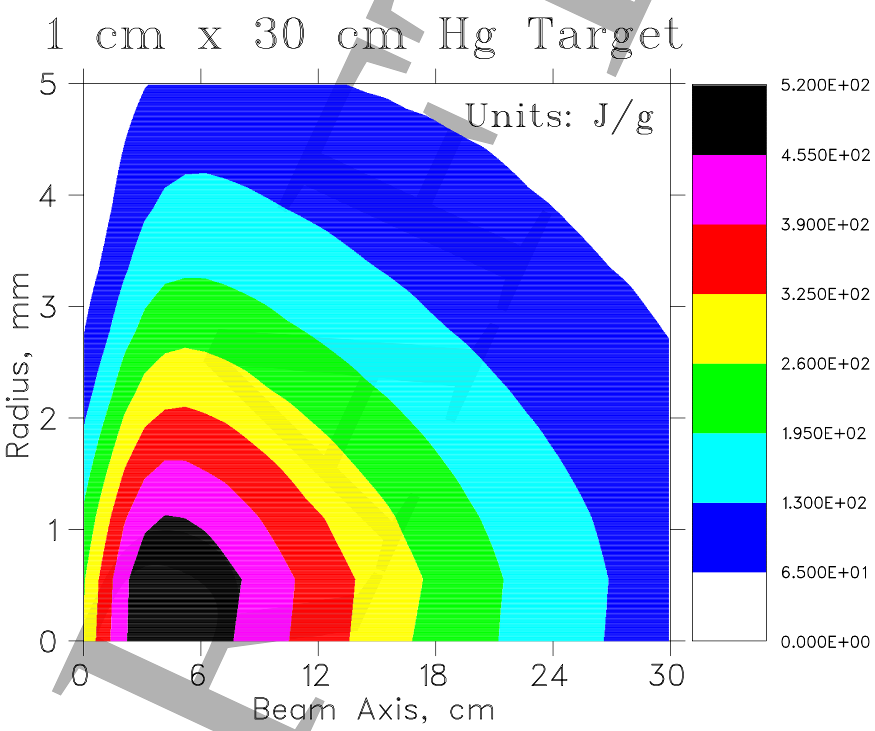

FIG. 2: Contours of energy deposition on a 5 mm radius and 30 cm length Hg target for a 1 MW, 2.5 Hz and 24 GeV proton beam

not so serious in the Fermilab case.

The capture solenoid is also assumed to be the same as in the muon collider status report[9]; it averages $B_z = 20$ T in the 30 cm of the target and it is followed by a field taper down to 1.25 T, which is a variation of that given by Y. Fukui[10]. Table III is the file for019.dat for the ICOOL run; it shows the position, length, and radii of the current

TABLE III: Target and matching section. Parameters of the 42 current sheets used in the simulation.

sheet number	position m	Length m	radius m	J A-turn/m	sheet number	position m	Length m	radius m	J A-turn/m
1	-0.433	.103	8.350001E-02	764999.8	22	1.326	.7099999	.7158333	2388100
2	-0.433	.103	.1005	764999.8	23	1.326	.7099999	.7635	2388100
3	-0.433	.103	.1175	764999.8	24	1.326	.7099999	.8111666	2388100
4	-0.433	.475	.1305	439200	25	2.086	.9590001	.936	1774800
5	-0.433	.475	.1395	439200	26	2.086	.9590001	.97	1774800
6	-0.433	.475	.1485	439200	27	2.086	.9590001	1.004	1774800
7	-0.433	.616	.1636667	776533.4	28	3.095	1.465	1.274167	1515834
8	-0.433	.616	.185	776533.4	29	3.095	1.465	1.3025	1515834
9	-0.433	.616	.2063333	776533.4	30	3.095	1.465	1.330833	1515834
10	-0.433	.755	.2308333	650166.6	31	4.61	3.153	1.507833	925898.5
11	-0.433	.755	.2585	650166.6	32	4.61	3.153	1.5235	925898.5
12	-0.433	.755	.2861667	650166.6	33	4.61	3.153	1.539167	925898.5
13	-0.708	.882	.4533333	4970667	34	7.813	4.707001	1.503833	565033.4
14	-0.708	.882	.56	4970667	35	7.813	4.707001	1.5115	565033.4
15	-0.708	.882	.6666667	4970667	36	7.813	4.707001	1.519167	565033.4
16	0.224	.517	.4386667	3688801	37	12.57	6.700001	1.502167	336865.6
17	0.224	.517	.516	3688801	38	12.57	6.700001	1.5065	336865.6
18	0.224	.517	.5933334	3688801	39	12.57	6.700001	1.510833	336865.6
19	0.791	.485	.5536667	3065332	40	19.32	6.700001	1.502167	336865.6
20	0.791	.485	.617	3065332	41	19.32	6.700001	1.5065	336865.6
21	0.791	.485	.6803333	3065332	42	19.32	6.700001	1.510833	336865.6

sheets. The following plots show an schematic of the target magnet first and then the field it generates; this field agrees quite well with that of an ideal field profile[11] (red) following the form: $B = \frac{B_o}{1+kL}$ where B_o is 20 T and $k = 0.778$.

C Phase Rotation No. 1

An early, high gradient, phase rotation is required if polarization is to be selected without particle loss. Forward decays, having one polarization, yield higher energy muons than backward decays which have the other polarization. At the end of this first stage, the bunch length has increased by a factor of 6 and the energy spread has decreased by the same

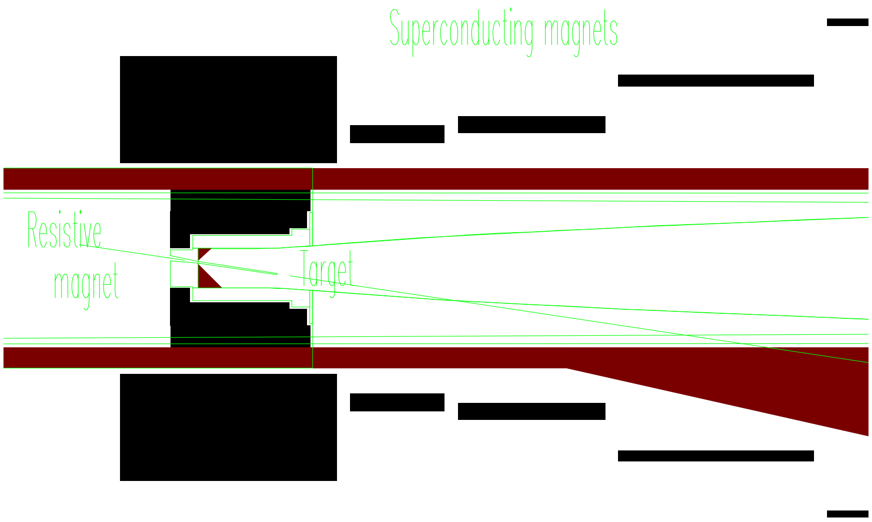

FIG. 3: Schematics of the target magnet

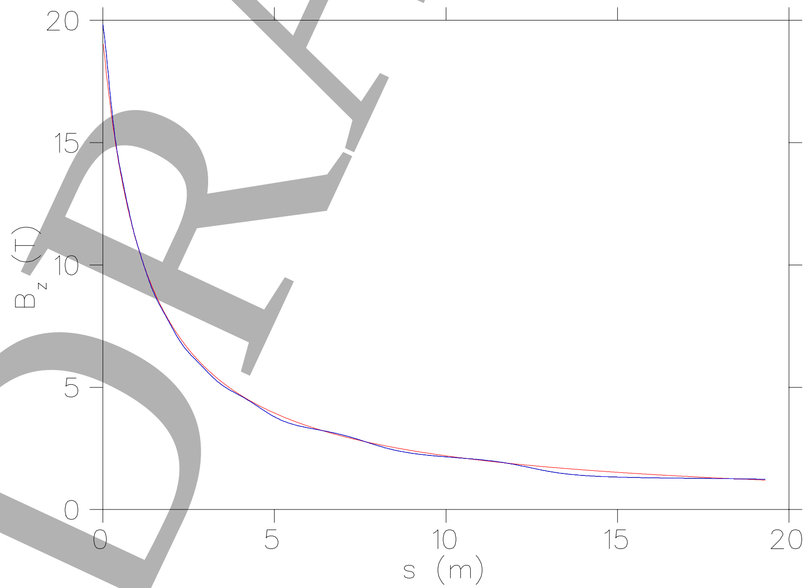

FIG. 4: Longitudinal B_z field at the front end. Actual magnetic field used in the simulations in blue; ideal tapering in red

amount. The following Tb.IV gives parameters obtained with an initial proton energy of

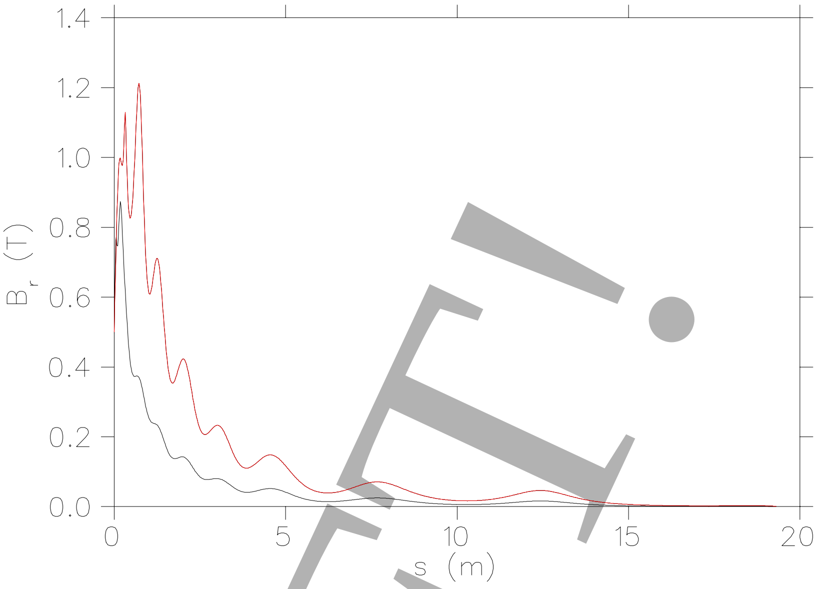

FIG. 5: Target region: radial magnetic field *vs.* distance z (m) at r=10 cm and 30 cm.

24 GeV. One can assume that for an initial energy of 16 GeV, the ratio of muons to protons would be 2/3 of the values shown. The performance numbers are given for the particles between a ct of -2.5 and + 6 m, they are: the number of μ/p is 50 %; $< p >=$ 283 MeV/c, *rms* σ_p = 42 MeV/c, *rms* σ_z = 1.89 m and the emittance is ϵ_{LN} = 0.856 π-m. It should be noted that this cut is not physical, is used only for the parameters in the tables and plots of the first phase rotation, and do not apply to the final muon plots. In addition, for the target, the sixth column refers to pions per protons rather than muons per protons.

At the end of this first phase rotation, the simulated energy *vs.* time distribution is shown in Fig.6. The blue dots show the muons within the cut and the ellipse fits 90 % of the particles in the cut.

D Mini Cooling

Mini-cooling reduces the muon energies so that the subsequent drift length for a second phase rotation could be kept short. It also lowers the transverse emittance.

The mini cooling was done in two hydrogen absorbers in a fixed magnetic fields of 1.25 T;

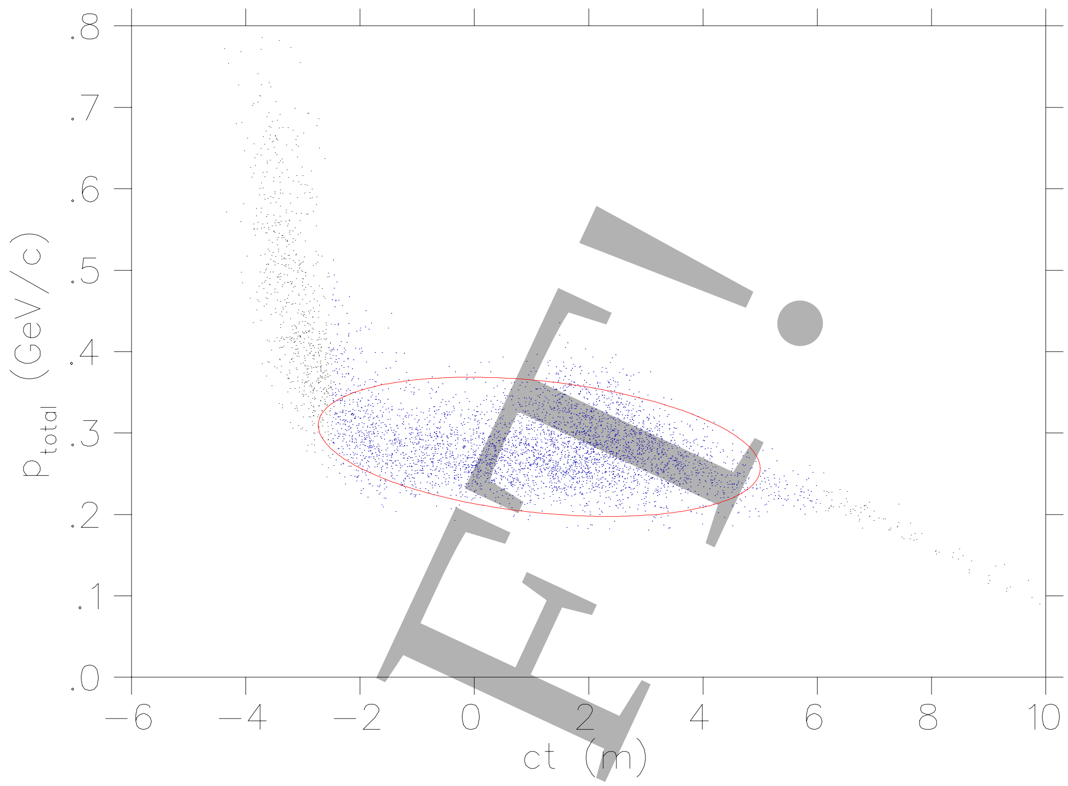

FIG. 6: Longitudinal phase space at $s = 47.8$ m, the end of phase rotation No. 1 after a cut at $ct = 10$ m. The number of μ/p is 65 %; $< p >= 307$ MeV/c, *rms* $\sigma_p = 86$ MeV/c and *rms* $\sigma_z = 2.45$ m

TABLE IV: Parameters of the first phase rotation.

	len	rad	B	f	grad	n_μ/n_p	σ_{ct}	$< p >$	$\sigma_p/ < p >$	ϵ_L
	m	m	T	MHz	MV/m		m	MeV/c	%	π m
target	.3	.03	20			1.15				
match	6.3	.6	1.25			0.6				
rf	12	.6	1.25	40	5					
rf	37	.6	1.25	30	5					
rf	5	.6	1.25	45	6	0.5	1.9	283	14.8	0.85

between the two, there is a matched field reversal in order to remove canonical angular momentum generated by the energy loss in the absorbers. The following figure shows the

TABLE V: Parameters of a mini-cooling cell

	len	rad	B	n_μ/n_p	σ_{ct}	$<p>$	$\sigma_p/<p>$	ϵ_L
	m	m	T		m	MeV/c	%	π m
mini-cooling 1	3.2	.3	1.25	.36	2.0	227	18	0.84
B reversal	16.1	.6						
mini-cooling 2	.7	.3	1.25	0.48	1.8	205	20	0.87

energy vs time after the mini cooling. As indicated before, the blue dots are within a $-2.5\ m \geq ct \leq +6\ m$ cut and the ellipse fits 90 % of the particles.

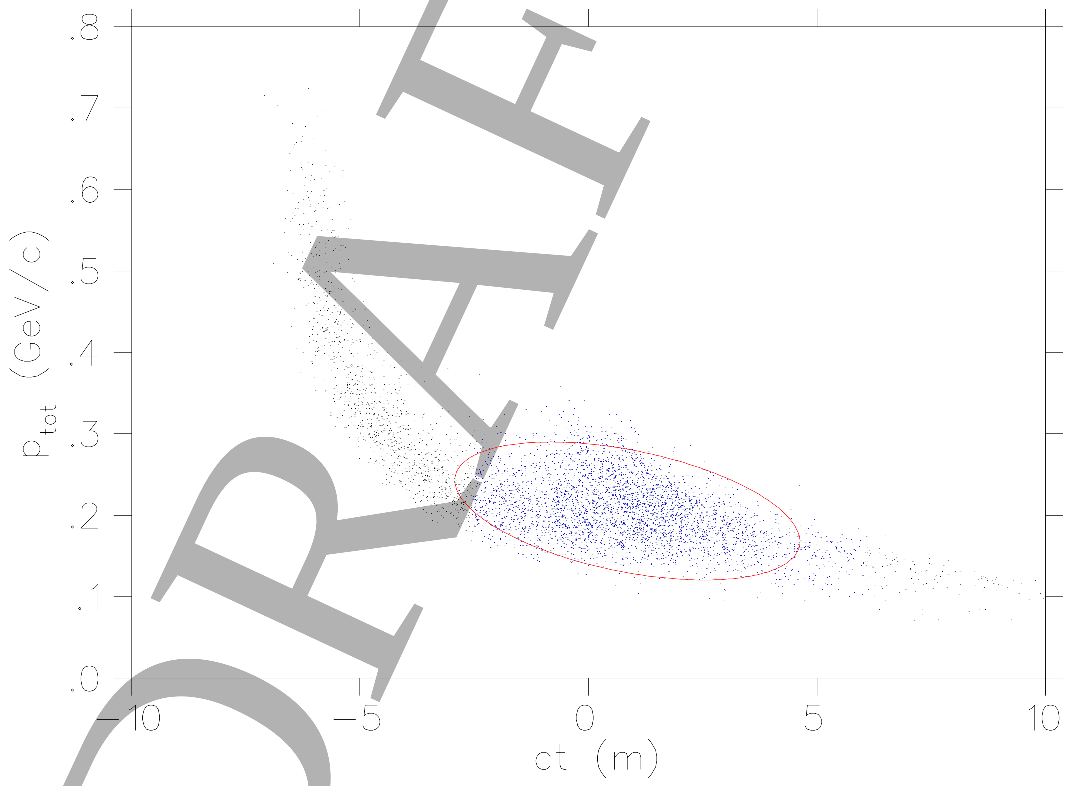

FIG. 7: Longitudinal phase space at the end of the mini-cooling section after a cut at $ct = 10$ m. The number of μ/p is 66 %; $<p>= 238$ MeV/c, *rms* $\sigma_p = 90$ MeV/c and *rms* $\sigma_z = 3.06$ m

E Phase Rotation No. 2

The object of this component is to further reduce the momentum spread at the expense of lengthening the bunch up to a distance of 90 m, approaching the initial proton bunch spacing ($\approx 135\ m$). The very long resulting bunch is then re-bunched at a higher frequency (175 MHz), yielding a train of about 50 individual muon bunches for every initial proton one. In addition, this second rotation results in the polarization being correlated with time, *i.e.* bunch number, instead of energy. The polarization is now preserved.

The rotation is performed by two drifts of 80 m and 50 m, respectively, with a field reversal between them (20 m), the field reversal is in order to control the growth of canonical angular momentum; this is followed by energy correction using an induction linac.

The coils used to reverse the fields are shown in Figs.8,9 and Tb.VI. Their current densities are low, but their radii are unnecessarily large, this need to be corrected. There should be even less problem in obtaining the desired field profile with smaller radius coils.

TABLE VI: Parameters of the 20 current sheets used to control the growth of canonical momentum.

sheet number	position m	length m	radius m	J A-turn/m	sheet number	position m	length m	radius m	J A-turn/m
1	-6.5	6.5	1.008333	334465.2	11	10.30069	.7	1.0125	-1409453
2	-6.5	6.5	1.025	334465.2	12	10.30069	.7	1.0375	-1409453
3	-6.5	6.5	1.041667	334465.2	13	12.37743	.65	1.0125	-867811
4	0	6.5	1.008333	334465.2	14	12.37743	.65	1.0375	-867811
5	0	6.5	1.025	334465.2	15	13.5	6.5	1.008333	-334465.2
6	0	6.5	1.041667	334465.2	16	13.5	6.5	1.025	-334465.2
7	6.972577	.65	1.0125	867811	17	13.5	6.5	1.041667	-334465.2
8	6.972577	.65	1.0375	867811	18	20	6.5	1.008333	-334465.2
9	8.999309	.7	1.0125	1409453	19	20	6.5	1.025	-334465.2
10	8.999309	.7	1.0375	1409453	20	20	6.5	1.041667	-334465.2

The β function in the field reversal region is shown in Fig. 10.

The induction linac (± 80 MeV acceleration) has a single pulse shape tailored to correct the time-energy correlation generated by the drift. It is simulated here by a sequence of

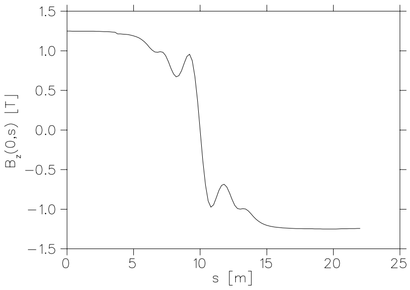

FIG. 8: Mini-cooling region: axial magnetic field *vs.* s (m).

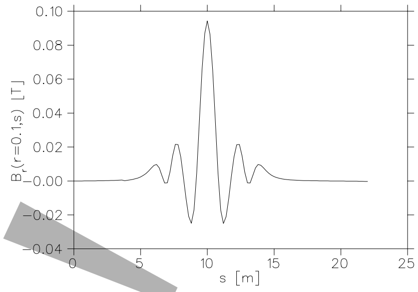

FIG. 9: Mini-cooling region: radial magnetic field *vs.* s (m) at r=10 cm.

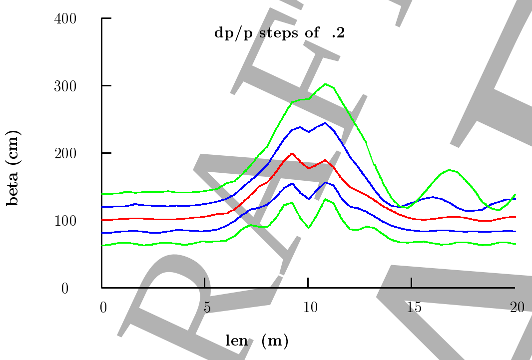

FIG. 10: β function in the region of field reversal.

sinusoidal rf fields. The induction linac must supply a rapid train of accelerations, spaced by the proton bunch spacing (135 m), and equal in number to the number of proton bunches. The wave form used is thus made up of harmonics (2.2, 4.4, and 8.8 MHz) of the bunch spacing (2.2 MHz).

The following figures show the momentum *vs.* the length of the muon bunch (c-time) before correction (Fig. 11), the energy change from the induction linac (Fig. 12), the momentum *vs.* c-time after the energy correction (Fig. 13), and the polarization *vs.* c-time (Fig. 14). In Fig. 11 the number of μ/p is 60 %; $< p >= 238$ MeV/c, *rms* $\sigma_p = 90$ MeV/c and *rms* $\sigma_z = 14.3$ m and in Fig. 13 the number of μ/p is 51 %; $< p >= 239.5$ MeV/c, *rms* $\sigma_p = 22.8$ MeV/c and *rms* $\sigma_z = 16.7$ m within a $-40 - +60$ m ct cut shown in blue.

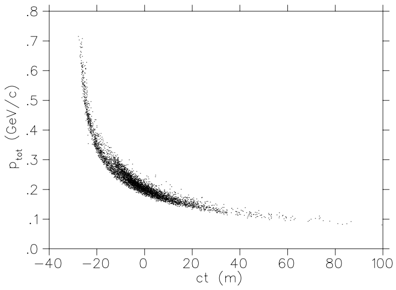

FIG. 11: Longitudinal phase-space at the end of the long drift (s=217.8 m).

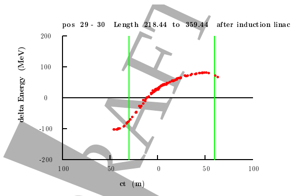

FIG. 12: Energy change *vs.* the length of the muon bunch (c-time)

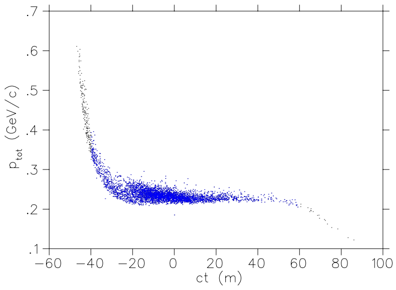

FIG. 13: Longitudinal phase-space at the end of phase rotation No. 2 (s=359 m).

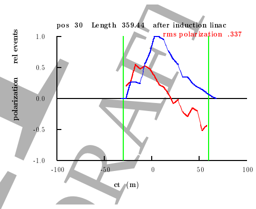

FIG. 14: Polarization *vs.* c-time (m)

The sensitivity of the maximum polarization and energy spread to the initial proton bunch length is shown in Fig. 15

In this simulation, the B field in the induction linac is taken as fixed at 1.25 T. However, higher fields may be preferred for induction linac cost and amplitude-energy correlation matching reasons.

F Matching into FOFO lattice

A sequence of solenoids is introduced to match the beta's from the fixed solenoid, of the phase rotation and induction linac, to a FOFO lattice. The coil details used are given in Tb.VIII and Fig.16; they are not realistic, their current densities are too high, but the B fields are reasonable and a suitable coil system will be designed after the focusing in the

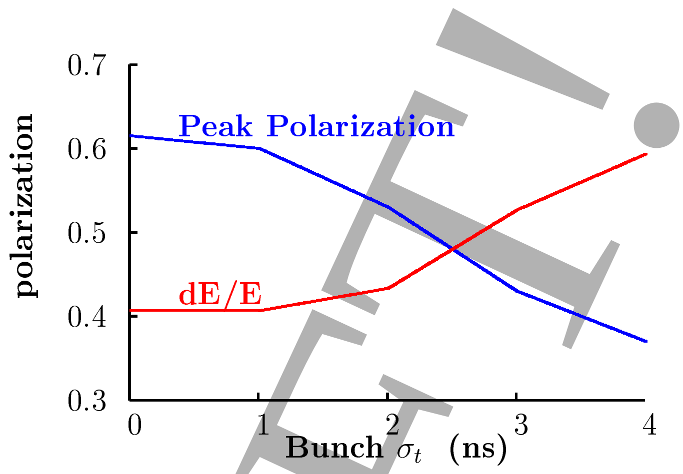

FIG. 15: Polarization and energy spread *vs.* the proton bunch length. *rms* polarization = 0.35 and dp/p intrinsic (*i.e.* with amp-mom correlation removed) =3.7

TABLE VII: Parameters of the phase rotation No. 2

	len	rad	B	freq.	grad	n_μ/n_p	σ_{ct}	$< p >$	dp/p	ϵ_{LN}
	m	m	T	MHz	MV/m		m	MeV/c	%	π m
drift 1	80	0.3	1.25			0.60				
B reversal	20	.6				0.60				
drift 1	50	0.3	1.25			0.60				
Ind Lin	141	0.3	1.25	2.2-8.8	$\pm$ 0.55	0.51	18	230	9.5	3.72

induction linac is established.

TABLE VIII: Parameters of the coils for the matching section.

`http://pubweb.bnl.gov/people/gallardo/pjk/for023.dat`

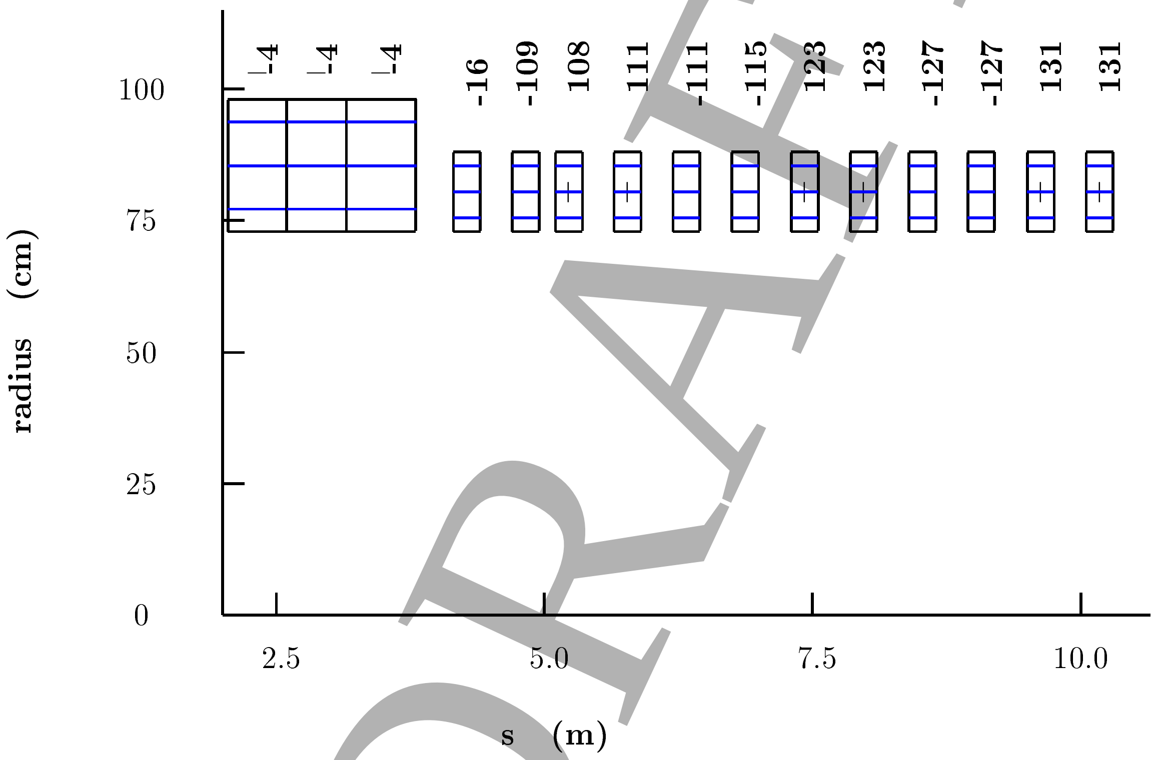

FIG. 16: Coil layout for the matching section

The B field in the matching and the beta function for a range of momenta are given in the Figs.17-19 below:

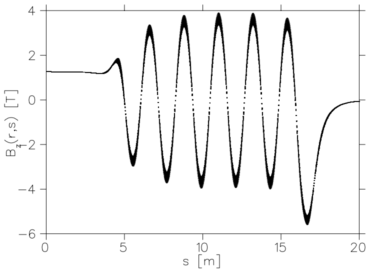

FIG. 17: Matching into the FOFO region: axial magnetic field *vs.* s (m) for several radial positions

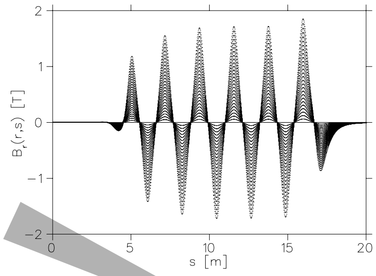

FIG. 18: Matching into the FOFO region: radial magnetic field *vs.* s (m) for several radial positions

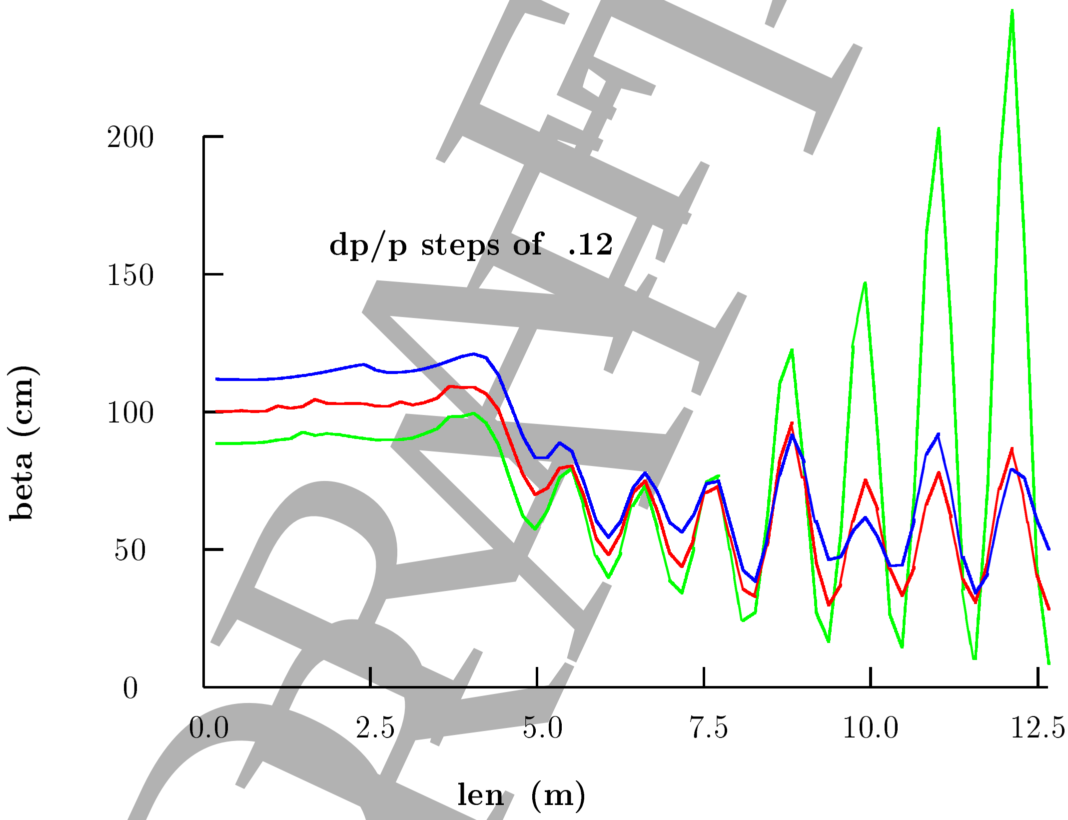

FIG. 19: Beta function in the matching to the FOFO section

G FOFO lattice

The same lattice is used in the bunching and subsequent cooling. The dimensions and current densities of the coils of 2 cells are in Tb. IX

TABLE IX: Coil parameters for a FOFO lattice

sheet number	position m	length m	radius m	J A-turn/m
20	3.576279E-06	.000001	1.075	1
21	.2500046	.6	.7716667	-4733333
22	.2500046	.6	.855	-4733333
23	.2500046	.6	.9383333	-4733333
24	1.100005	.000001	1.075	-1
25	1.350006	.6	.7716667	4733333
26	1.350006	.6	.855	4733333
27	1.350006	.6	.9383333	4733333
28	2.200006	.000001	1.075	1

These coils and B fields on axis for the FOFO are shown in the following Figs.20-21 and the β function for a range of momenta are in Fig. 22

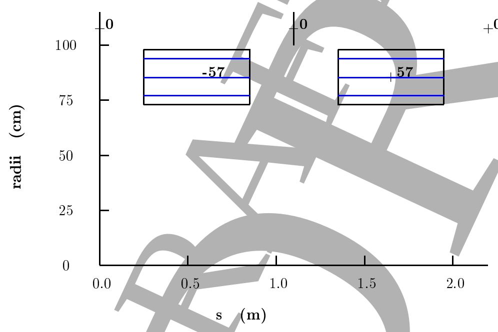

FIG. 20: Schematic of one cell of the FOFO lattice

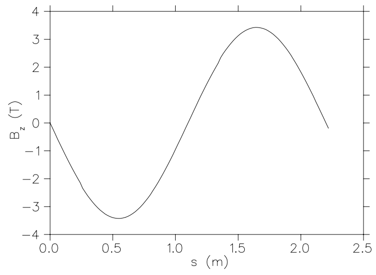

FIG. 21: FOFO region: axial magnetic field *vs.* distance z (m)

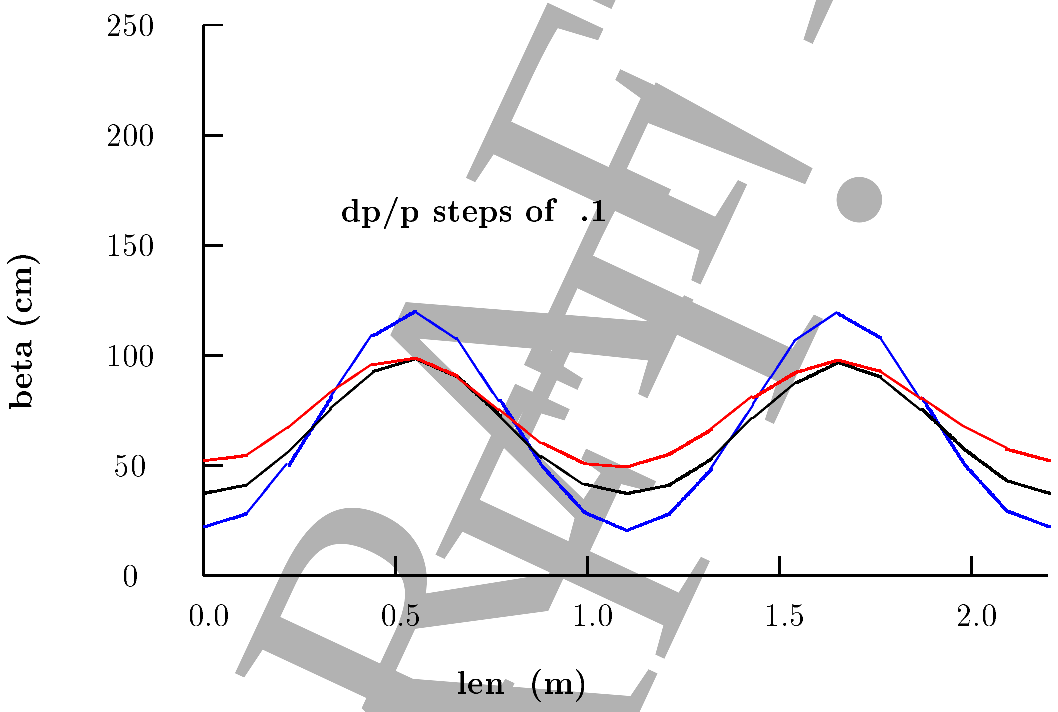

FIG. 22: β function in one cell of the FOFO lattice for different momenta

H Bunching

Bunching is performed in two stages, each consisting of 175 MHz rf, second harmonic (350 MHz) rf, and a drift. The frequencies used are chosen to be a multiple of 350 MHz, the frequency of the LEP super-conducting cavities that are assumed to be used in the later acceleration. The 175 MHz cavities are placed at the high beta locations, just as in the cooling (see below), but the 350 MHz cavities are at the beta minima, where the hydrogen absorbers are in the cooling. Two cells are used for rf in the first stage, followed by a first drift (21 m). 3 cells are used for rf in the second followed by the second drift (11 m). The arrangement is illustrated in Fig.23

Momentum *vs.* ct (modulo one wavelength) and the rf induced changes of energy are

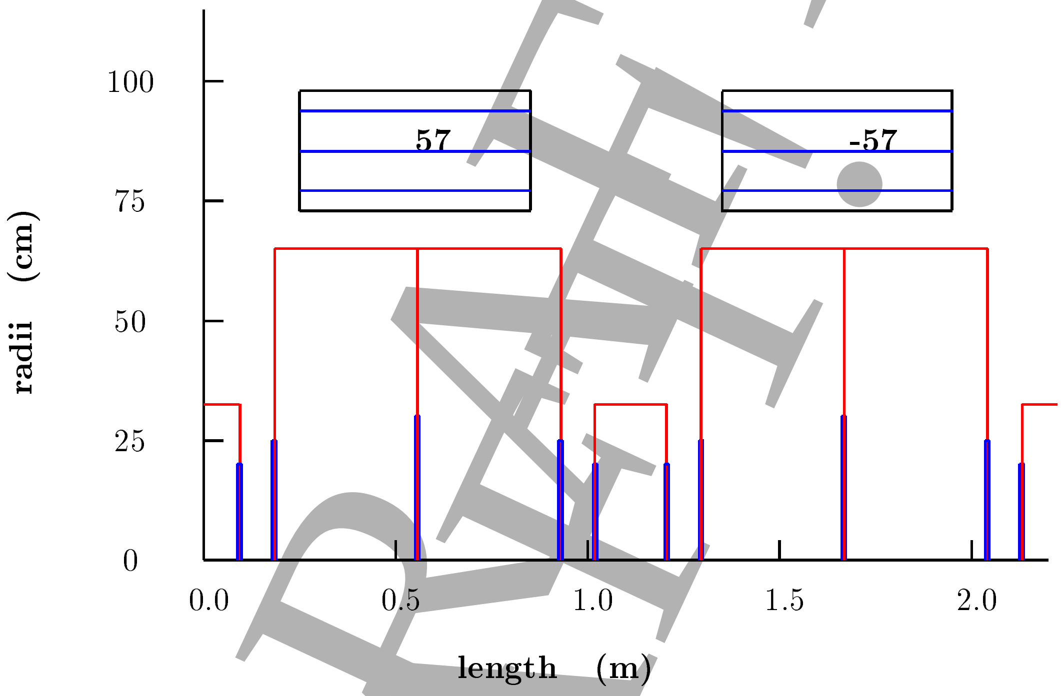

FIG. 23: One period of the bunching section lattice

TABLE X: Parameters for the bunching section

frequencies	175 and 350 MHz
gradients	8 MV/m and 6.66 MV/m
drifts	19 and 10 m
bunches formed	52
initial rms dp/p	3.6 %
final rms dp/p	9 %

shown in: Fig.24, at the entrance of the first drift the number of $\mu' s$ per proton is 0.49; $\sigma_z = 47\ cm$, $\sigma_p = 14.5$ MeV/c, $< p >= 236.2$ MeV/c and $\epsilon_L N = 64.5\ \pi$ mm. After the drift, Fig. 26, the number of $\mu' s$ per proton is 0.48; $\sigma_z = 46\ cm$, $\sigma_p = 16.9$ MeV/c,

$< p >= 235.4$ MeV/c and $\epsilon_L N = 73.6\ \pi$ mm. After the first bunching section, Fig. 27, the number of $\mu's$ per proton is 0.47; $\sigma_z = 47\ cm$, $\sigma_p = 23.5$ MeV/c, $< p >= 235.5$ MeV/c and $\epsilon_L N = 104.5\ \pi$ mm. This is follows by a second drift, at the end, Fig. 29, the number of $\mu's$ per proton is 0.47; $\sigma_z = 47\ cm$, $\sigma_p = 23.5$ MeV/c, $< p >= 235.5$ MeV/c and $\epsilon_L N = 104.5\ \pi$ mm. Finally, at the end of the second bunching section, Fig. 30,the number of $\mu's$ per proton is 0.45; $\sigma_z = 23.4\ cm$, $\sigma_p = 23.2$ MeV/c, $< p >= 232$ MeV/c and $\epsilon_L N = 51\ \pi$ mm.

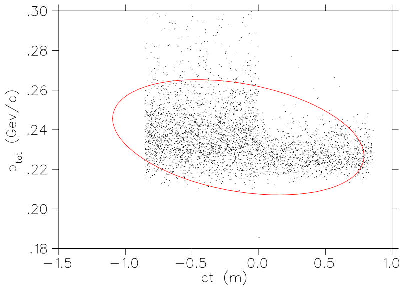

FIG. 24: Longitudinal phase space at the first drift (s=369.45 m)

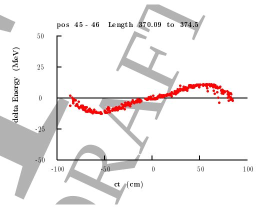

FIG. 25: Change of energy *vs.* c-time

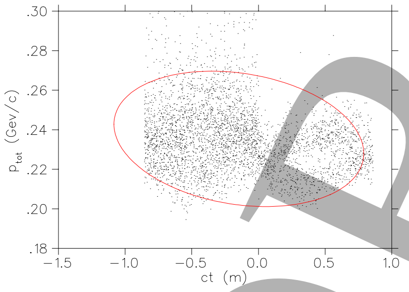

FIG. 26: Longitudinal phase space after the first drift (s=373.85 m)

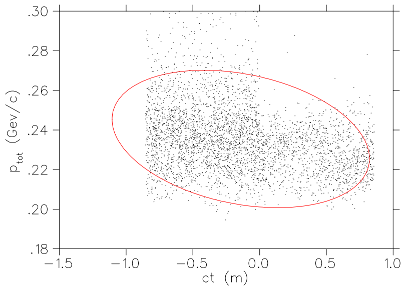

FIG. 27: Longitudinal phase space after the first bunching section (s=394.76 m)

I Cooling

A simple comparison of the total produced six dimensional emittance and the total acceptance of a plausible storage ring indicates that cooling might not be needed. But with-

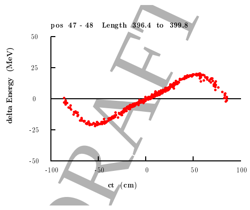

FIG. 28: Energy change *v.s.* c-time

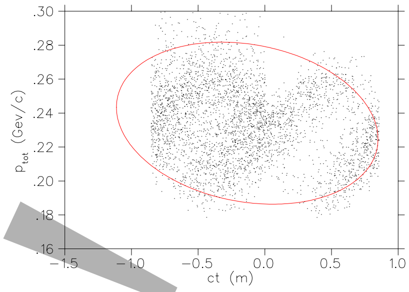

FIG. 29: Longitudinal phase space after the second drift (s=399.16 m)

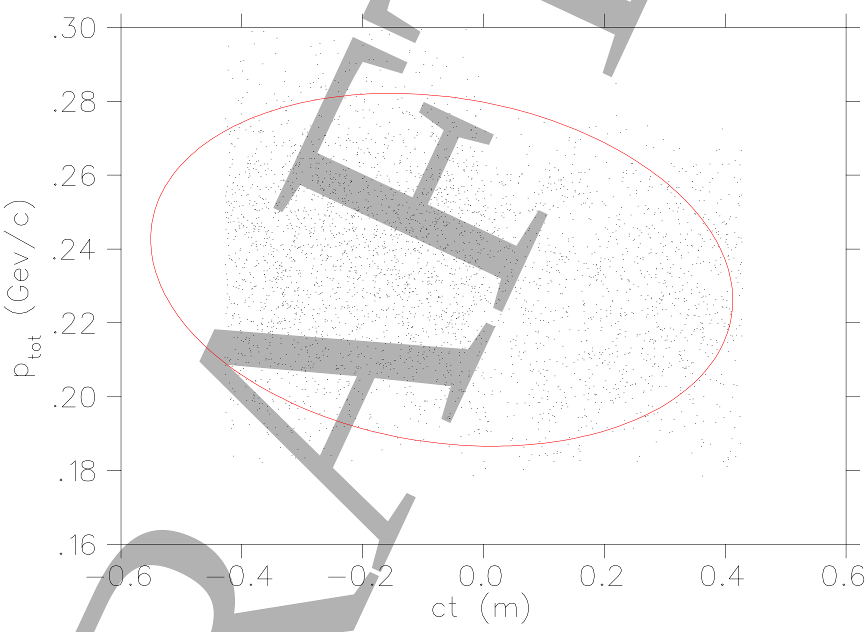

FIG. 30: Longitudinal phase space at the end of the buncher (s=409.1 m)

out cooling, the muon accelerator would have to have a transverse acceptance of about 100 π mm rad. This, as we have shown, is possible with large aperture solenoid focusing and low frequency rf, but would be difficult and expensive for the accelerator.

A more reasonable acceleration scheme might have a transverse acceptance of 15 π mm rad, and a longitudinal acceptance of 140 π mm (= 0.05 eV s). The following cooling is designed to match into this acceptance.

The current simulation, using a fixed lattice, cools to $\approx$ 3.5 π mm rad. This is larger than

TABLE XI: Parameters for one cell of the cooling section

		part No. 1		part No. 2	
Length		28 m		46 m	
	mat	length	radius	length	radius
		cm	cm	cm	cm
Absorber	H	14	20		
window	Al	.04	20		
space		10.7			
rf window	Be	.025	25	.0125	20
rf gap		37.3	65		
rf window	Be	.05	30	.025	25
rf gap		37.3	65		
rf window	Be	.025	25	.0125	20
space		10.7			
window	Al	.04	20		

the originally specified 1.5 π mm rad in [1], but because the distributions are truncated, a high fraction of the beam is accepted into 15 π mm rad. The coils have been shown before and the rf gradients are 14 MV/m. The absorber, windows and rf dimensions are shown in Tb.XI

This is illustrated below:

The transverse and longitudinal emittances *vs.* distance are:

The emittances are plotted in Fig.32

1. with no cuts,

2. with transverse acceptance cuts at 13.5, 9.35, and 6 π mm rad.,

3. with the same transverse cuts together with a longitudinal cut at 71 π mm.

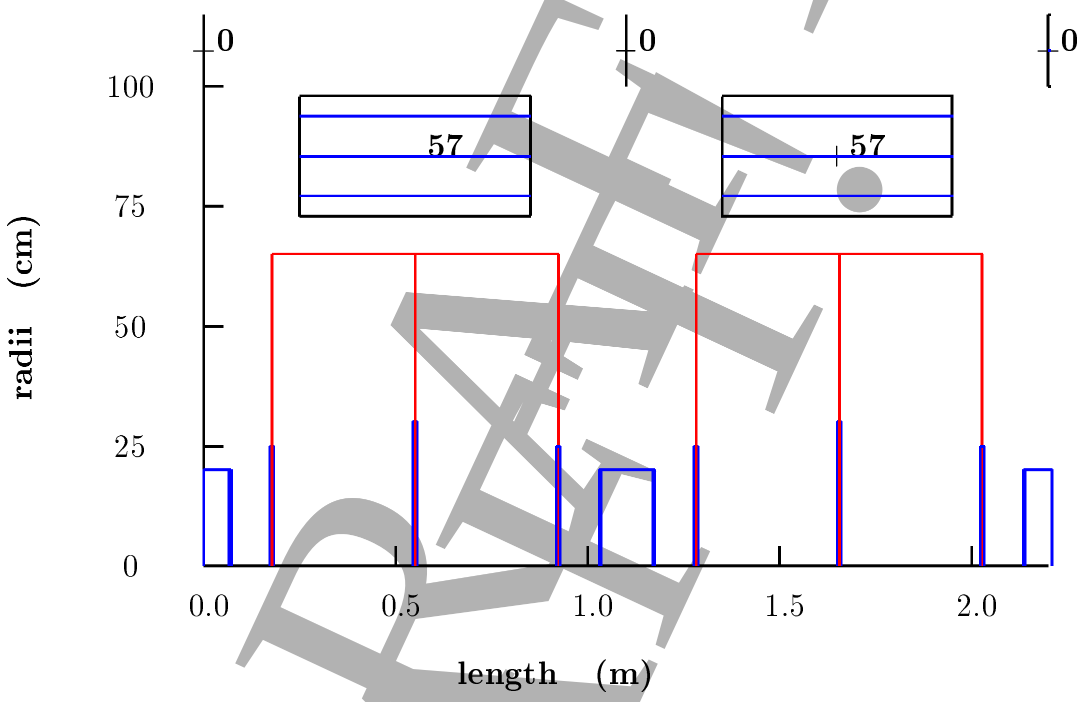

FIG. 31: Cooling cell

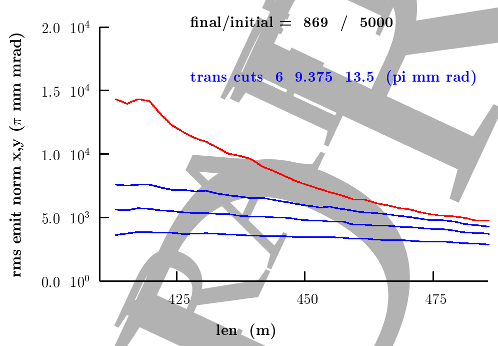

FIG. 32: Transverse emittance *vs.* distance z (m)

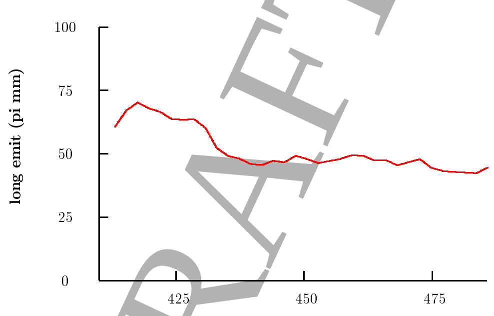

FIG. 33: Longitudinal emittance *vs.* distance z (m)

These emittances are all significantly larger than that previously estimated for the PJK[1] front end (1.5 π mm rad). Further cooling reduces the emittance, but is found to also reduce the number of muons accepted by the accelerator. In this example, the cooling length was chosen to maximize the number of muons accepted into 6 π mm rad transverse, and 71 π mm longitudinal phase space. See below:

The muons per initial proton are shown in Fig.34.

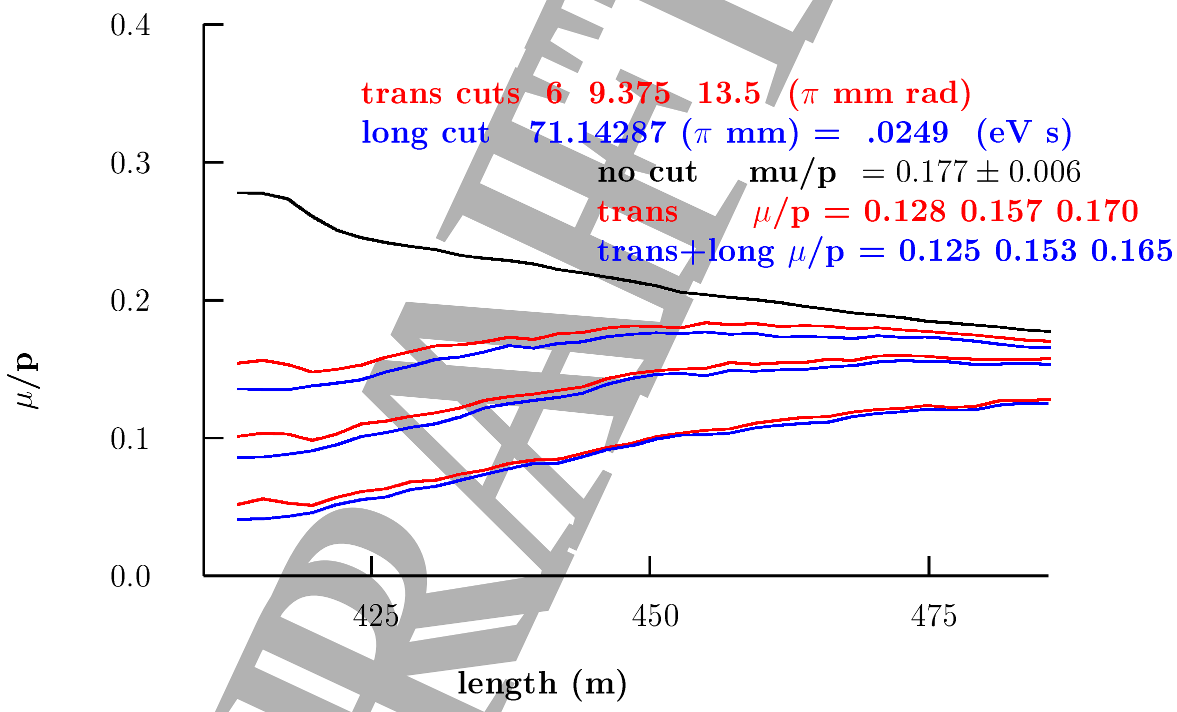

FIG. 34: Ratio $\frac{\mu}{p}$ vs. distance z (m)

III. SUMMARY

A Plots *vs.* length

The following plots show the values of some representative parameters as a function of length through the full system.

The axial field and radial fields has been shown before; in Fig.4 the axial field starts at 20 T and is tapered down to 1.25 T at about (≈ 18 m); the radial field is in Fig.5. The field is reversed in the middle of the minicooling section and reversed back again in the drift that follow, this is shown in Figs. 8-9. After the match into the FOFO in Fig. 17-18, with its $\pm$ 3.4 T fields, the fields are only plotted for one period of the FOFO cell in Fig. 21.

Figure 35 shows the rms beam radius and maximum particle radii. Both are seen to rise during the field taper and remain approximately flat in the phase rotations section, but rise and fall in the two matched field reversals where the beta functions are larger. After the beam is matched into the FOFO channel, the radii are only shown between the cells, at the centers of the absorbers, where the beta function is at a minimum. Because of this smaller beta, the rms beam radius is substantially reduced. In the cooling section it is further reduced by about a factor of two as the emittance is reduced. FIXME

In the rms momentum plot Fig. 36, the red line indicates rms momenta with cuts applied after the first phase rotation to select the rotated particles and to reject the tail of unrotated high, and very low, ones. This cut is not a physical one. The blue curve gives the larger spread of all the particles including the tails. DESCRI.

The rms emittance in Fig.38 is seen to drop rapidly in the first few meters as the acceptance of the channel cuts off large transverse momentum pions. It is reduced in the mini cooling, although there is clear evidence of some emittance blow up in the field reversal. The emittance then remains conserved until the cooling, where it drops as expected. FIG. 33

The μ/p plot Fig. 39 shows the loss of particles in the mini-cooling as the lowest energy pions are stopped in the hydrogen. The losses in the drift and induction linac are almost entirely from decays. The early step in number of muons after the start of the cooling come from the scraping of bunch tails remaining after the buncher. Later, straggling in the absorbers would cause the longitudinal emittance to grow, but since the bucket is already full, this leads to the steady loss observed.

In the average energy plot Fig. 40 one sees a consistent difference between the average and the reference momenta. This arises because of the slower forward motion of large amplitude tracks that is matched by a zero amplitude reference at a lower energy. At the end, as the cooling reduces the amplitudes, this difference is seen to go away.

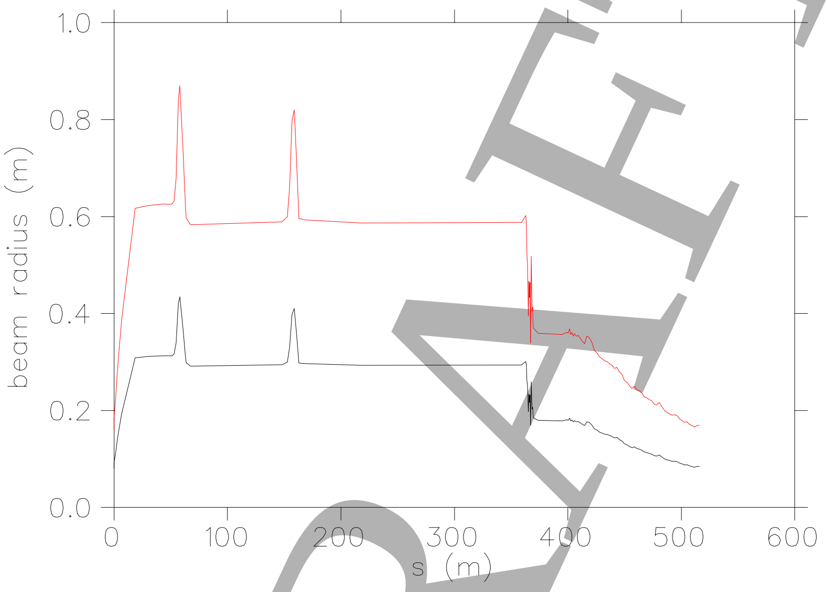

FIG. 35: *rms* beam radius blue and maximum beam radius red *vs.* distance z (m)

B Energies of pions used

In this plot we show the distribution of initial pion kinetic energies. In black, the distribution is for all initial pions, while in blue the distribution is only of those initial pions that made muons present at the end of the system. The red line shows the ratio of these two, *i.e.* the efficiency of muon production as a function of the initial pion energies. It is seen to span approximately from 50 to 450 MeV, with an efficiency in this range of about 20 %,

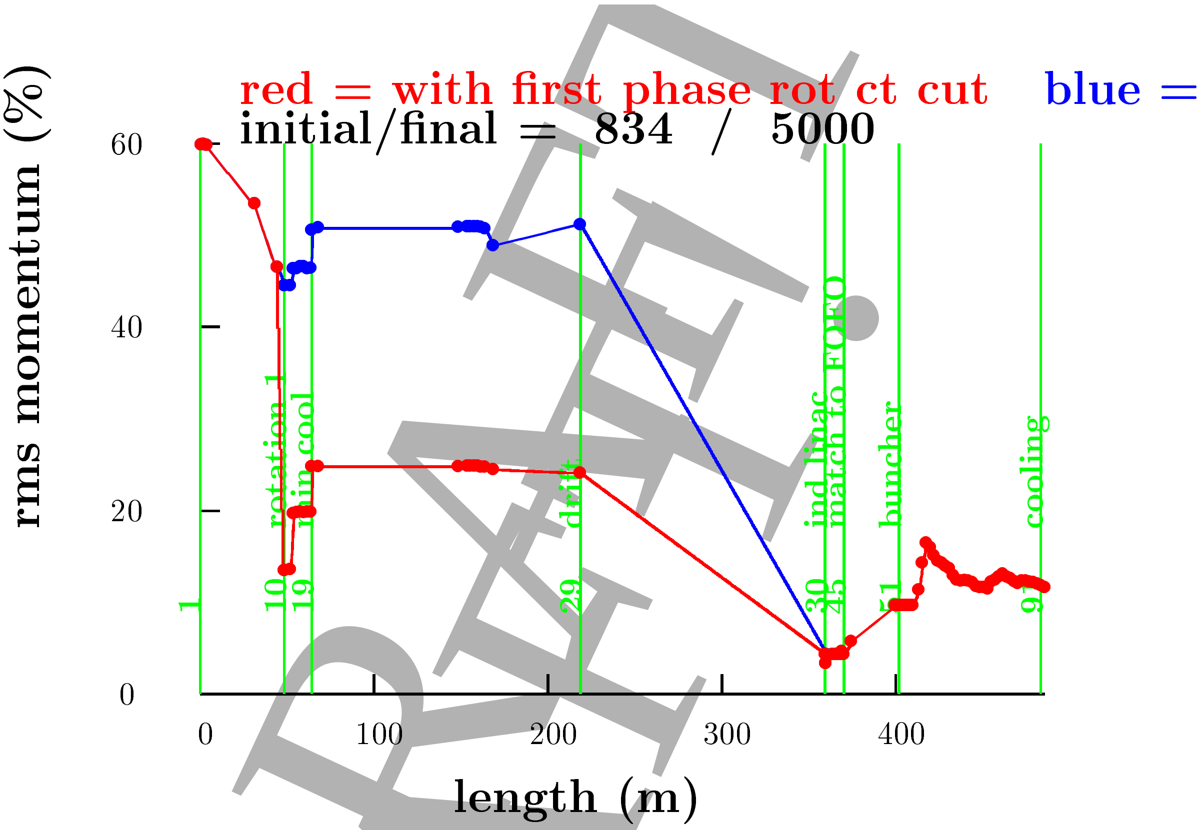

FIG. 36: *rms* momentum *vs.* distance z (m)

with a tail of used pions to 700 MeV.

C Comparison with other systems

Compared with the estimated performance of such a system in the PJK paper[1] and the Parameters Document[13], the number of muons per proton is a little higher (0.17 compared with 0.13), the longitudinal emittance is about the same ($\approx 31\ \pi$ mm), but the transverse emittance is larger ($3.9\ \pi$ mm rad. compared with $1.5\ \pi$ mm rad.). Thus, this study, using ICOOL, substantially confirms the earlier, but less accurate estimate.

We have also run ICOOL on a sequence of other systems, all using the same cooling and approximately the same induction linac acceleration voltage swing. These studies were

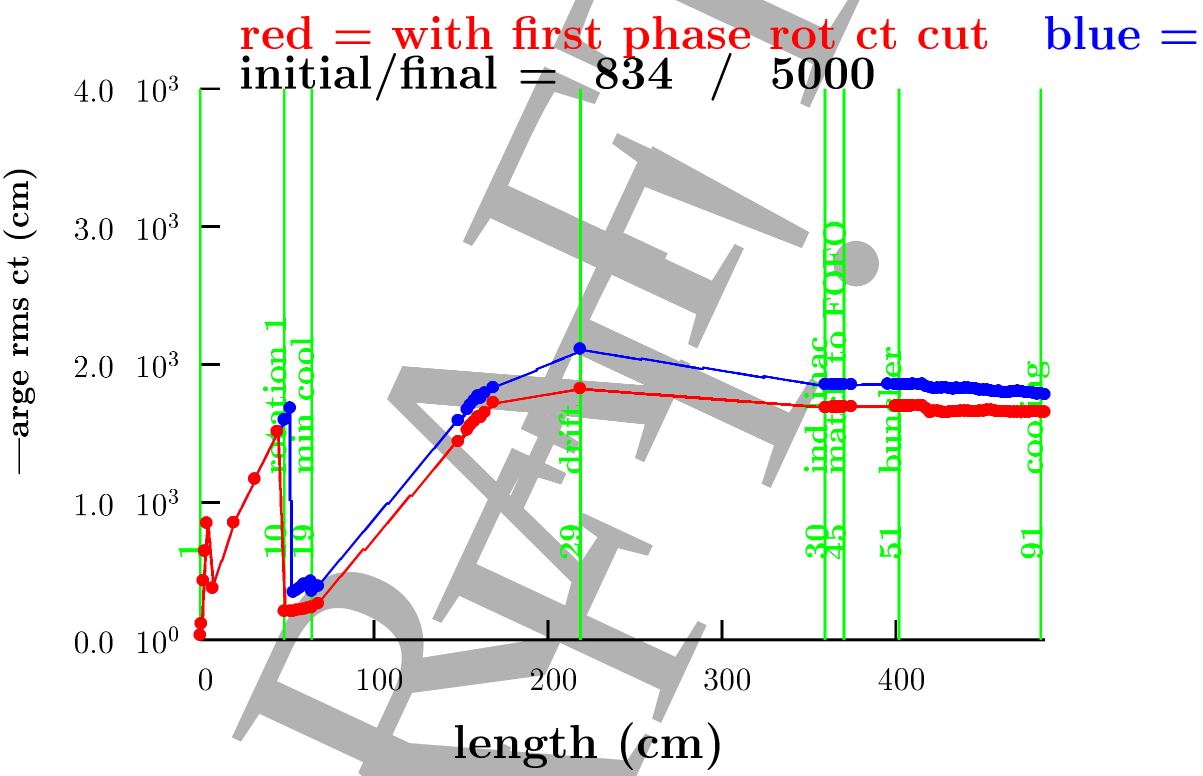

FIG. 37: *rms* c-time *vs.* distance z (m)

not optimized and thus the comparisons with them may favor the *base* example that is the subject of this paper.

The following table Tb.XII gives the approximate factors, and their cumulative effect, as various modifications are made to the above system: The factors have statistical accuracies of ≈ 7 %, and, in the final two entries, much larger possible dependencies on the details of the examples studied. Also given, are the number of muons per proton and the numbers of muon decays per year achieved with 1 MW proton drivers. It is assumed that 40 % of the storage ring circumference is used, and that the acceleration efficiency is 80 %. It is noted FIXME that the performance of the last example, which shares many features with the Feasibility Study case[12], has achieved the same number of muons per proton (0.015 μ/p). With the changes described below we may hope to raise the efficiencies of any of these examples by

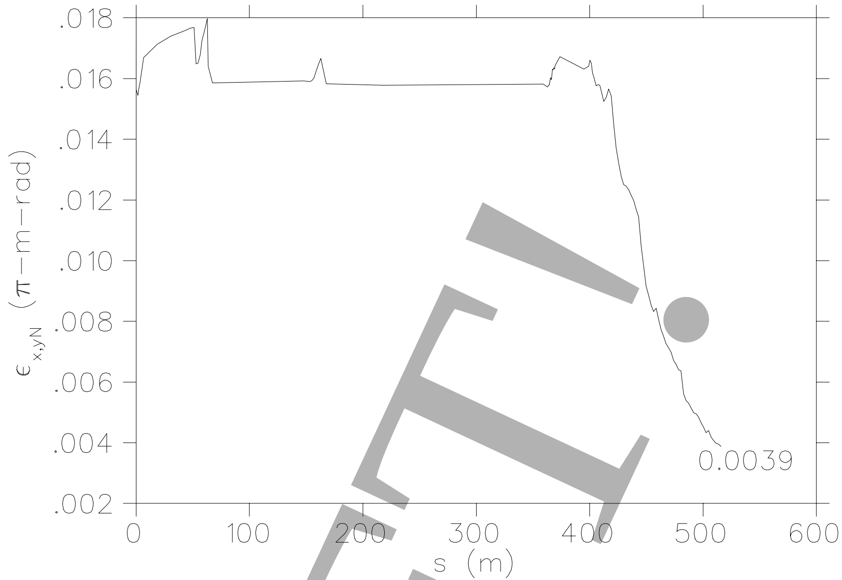

FIG. 38: *rms* normalized emittance *vs.* distance z (m)

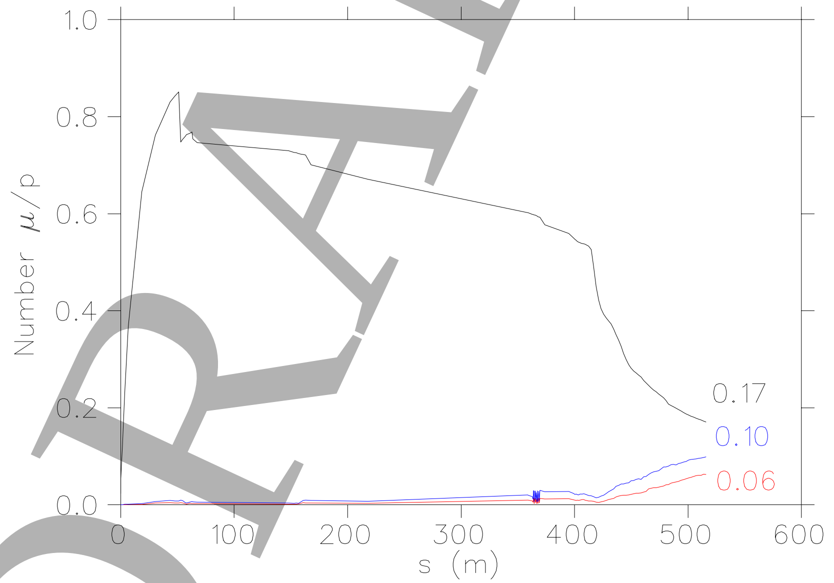

FIG. 39: $\frac{\mu}{p}$ *vs.* distance z (m)

as much as a factor of two, but the ratios between them are probably going to persist.

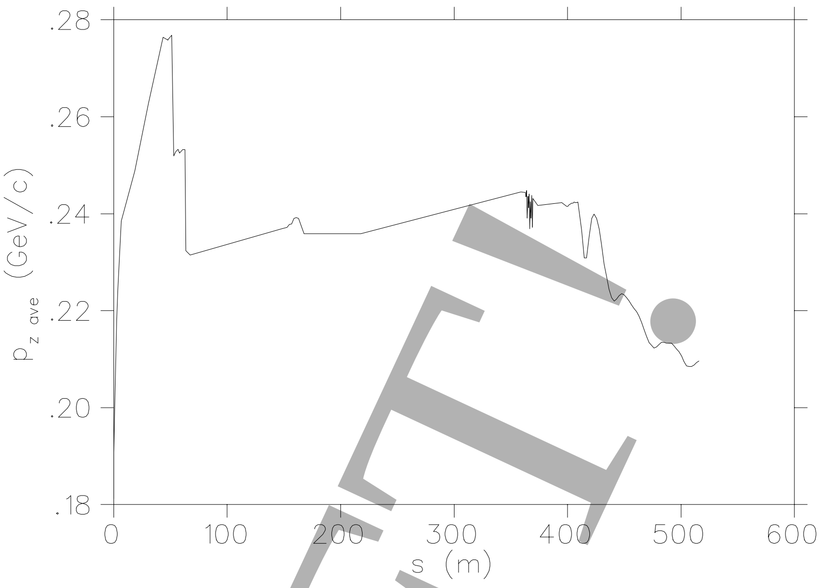

FIG. 40: Average momentum P_z *vs.* distance z (m)

D Possible changes and improvements

- Mercury Target

  As noted in the target section, the mercury target simulated here would probably not survive for the required 2μs of spill at the BNL-AGS at 1 MW (10^{14}), although it might well be OK with the smaller number of protons per spill (2.5×10^{13}) in Fermilab. Two ideas have been considered:

  1. deliberately blow up the emittance of the proton beam and focus it towards the back of the target.
  2. have four/six separate 3 mm beams side by side. *e.g.* 6 beams spaced by 1.2 cm (center to center) for a total spread of 6 cm. The proton beam is then swept across them so that only one bunch enters each target. FIXME

  Item 1) might reduce the temperature by a factor of 2-4; 2) reduces it by 6, and the resulting temperature rise would then be around 200-400 degrees, which is almost certainly acceptable. Conceivably, either item 1) or 2) might suffice alone.

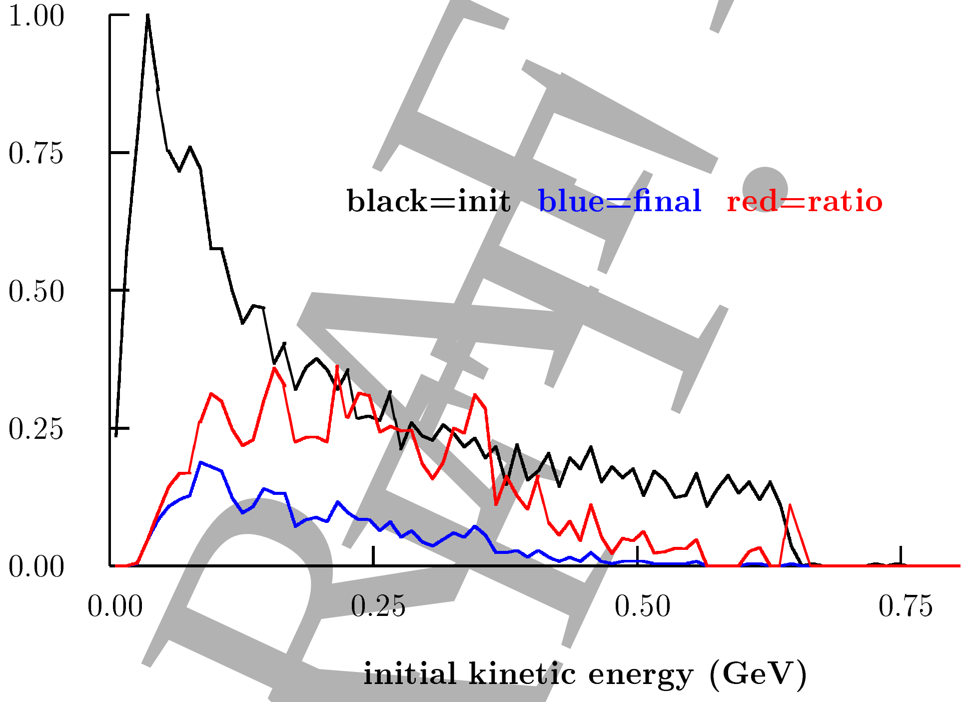

FIG. 41: Normalized energy distribution of initial muons (black), final muons (blue) and ratio $\frac{\text{final}}{\text{initial}}$

- Taper down from 20 T. The taper used falls to 1.25 T in about 6 m. This is theoretically too fast for the highest pion momenta captured ($\approx$ 700 MeV). It may be advantageous, therefore, to use a slower taper.

- Improved field reversal

  It was noted above that there is considerable particle loss in the field reversal between the absorbers of the mini-cooling, but little loss in the field reversal in the second phase rotation drift. This must be understood, and may require redesign of the first reversal.

- Match amplitude momentum correlation

TABLE XII: Comparison factors to results of similar systems

Change	factor mu/MW	cumulative	μ/p	μ decays/year
80 MHz rf to 3 m from target	1.07	1.07	0.16	1.3×10^{20}
Base	**1.0**	**1.0**	**0.15**	1.2×10^{20}
increase σ_t from 1 to 3 ns	.7	.7	0.105	0.85×10^{20}
change p energy 24 to 16 GeV	1.0	.7	0.07	0.85×10^{20}
remove first phase rotation	0 .5	.35	0.035	0.42×10^{20}
change target Hg to C	0.6	.21	0.021	0.25×10^{20}
shorten drift to 50 m	0 .6	.13	0 .015	0.16×10^{20}

Large amplitude particles, of a given momentum, have longer paths, and lower forward velocity, than low amplitude particles. In order to propagate in an rf lattice, such as the cooling channel, the large amplitude particles must have higher momentum than the lower ones, *i.e* a finite correlation is needed between amplitude and momentum. Such a correlation arises naturally in the phase rotation, and could, in principle have the required value for the cooling; but such is not the case here. The correct correlation could be obtained in various ways, the simplest of which would be to raise the axial magnetic field in the drift and linac. If this were done, transmission should be improved.

- Undistorted second phase rotation

  If phase rotation is achieved by a simple drift followed by a linac with fixed pulse shape, as was done in the second case here, then relativistic effects cause the rotated energy spread to be larger at short times (from initial high energies) and smaller at later times (from low initial energies). This effect can be clearly seen in Fig.30. As a result, the bunched rf buckets are overfilled by the early muons and under filled by the later ones. This distortion can be removed if at least two different linac pulse shapes are used[16]. The use of such non distorting phase rotation should improve transmission after the bunching.

- Increase cooling longitudinal acceptance

  The cooling channel used here has an effective acceptance of about 70 π mm, and there are few particles with amplitude above this. Yet the accelerators designed for the Feasibility Study are claimed to accept 140 π mm, which would be excessive for this case. One could either:

  1. reduce the acceptance of the accelerators, and thus reduce their cost; or
  2. use a cooling channel with larger acceptance (as was done in Balbekov's paper[14], and gain transmission of muons.

IV. CONCLUSION

The physics study[15] concluded that to do the most interesting known physics, one needs a muon storage ring yielding 2×10^{20} muons per year decaying in a straight section facing a detector. Although, with a 1 MW proton source, the current design falls somewhat short of this (1.2×10^{20}), we conclude that the desired 2×10^{20} is probably achievable with the further improvements described above. The physics report notes that for the expected oscillations, polarization is not strictly needed. However, if there are unexpected effects, as one would wish, the ability to use polarizations to change the ratio of μ and e neutrinos could become an essential feature in determining the nature of the new effect. But it is clear that to reach such a performance, one may need all possible features that increase efficiency. Whether such features increase the total cost is unclear, but they certainly demand significant R & D.

REFERENCES

[1] R. B. Palmer, C. Johnson and E. Keil, *A Cost Effective Design for a Neutrino Factory*, BNL-66971, CERN SL/99-070 AP, Neutrino Factory Note 0.9; also as a Muon Collider Note muc0067
http://www-mucool.fnal.gov/mcnotes/muc0067.ps

[2] Contribution to the Proceedings can be found at
http://muonstoragerings.cern.ch/Welcome.html (follow the links to Neutrino Factory and Workshop)

[3] Earlier runs of MARS were used in this study.

[4] J. C. Gallardo and R. B. Palmer, *MCM: Fortran program to simulate the front end and cooling section*, unpublished

[5] R. Fernow, *Fortran program to simulate front end and muon ionization cooling*

[6] N. V. Mokhov, *The MARS Code System User's Guide, Version 13(95)*, Fermilab-FN-628 (1995); N. V. Mokhov et al., Fermilab-Conf-98/379 (1998); LANL Report LA-UR-98-5716 (1998); nucl-th/9812038 v2 16 Dec 1998;
http://www-ap.fnal.gov/MARS/.

[7] N. V. Mokhov, *‘π/μ Yield and Power Dissipation for Carbon and Mercury Targets in 20-Tesla Solenoid with Matching Section”*, Mucool Note MUC0061 (1999),
http://www-ap.fnal.gov/mokhov/mumu/target99/muc0061 and updates there.

[8] H. Kirk, unpublished,
http://pubweb.bnl.gov/people/kirk/xxxxx

[9] C. Ankenbrandt, *et al.*, *Status of Muon Collider Research and Development and Future Plans*, Phys. Rev. **Accel. Beams**, 2, 081001 (1999).

[10] Y. Fukui, *Simulation of the pre-cooling stages of the neutrino factory*, Muon Collider Note muc0055

[11] R. Chehab, *Positron Sources*, LAL/RT 92-17 (1992); Ph. Royer, *Solenoidal Optics* and

references therein, http://nicewww.cern.ch/m̃olat/neutrino/nf11.pdf

[12] N. Holtkamp and D. Finley: editors, *A Feasibility Study of a Neutrino Factory Based on a Muon Storage Ring*,

`http://www.fnal.gov/projects/muon_collider/nu-factory/fermi_study_after_april1st/`

[13] R.B. Palmer, *Draft Parameters of a Neutrino Factory*, http://pubweb.bnl.gov/people/palmer/nu/params.ps

[14] V. Balbekov, *New Design of Alternate Solenoid Cooling Channel for Neutrino Factory*, Muon Collider Note muc0098 http://www-mucool.fnal.gov/mcnotes/muc0098.ps

[15] S. Geer and H. Schellman, *Physics at a Neutrino Factory: Draft No.2*, http://www.fnal.gov/projects/muoncollider/nu/study/study.html.

[16] R.B. Palmer, *Non-distorting phase rotation*, http://www-mucool.fnal.gov/mcnotes/muc0114.ps